

## **Supporting Information**

### One-Dimensional Supramolecular Nanoplatfoms for Theranostics Based on Co-Assembly of Peptide Amphiphiles

Inhye Kim,<sup>†</sup> Eun Hee Han,<sup>‡</sup> Jooyeon Ryu,<sup>†</sup> Jin-Young Min,<sup>†,‡</sup> Hyungju Ahn,<sup>§</sup> Young-Ho Chung,<sup>‡</sup> and Eunji Lee<sup>\*,†</sup>

Correspondence to: [eunjilee@cnu.ac.kr](mailto:eunjilee@cnu.ac.kr)

---

<sup>†</sup>Graduate School of Analytical Science and Technology, Chungnam National University, Daejeon 305-764, Republic of Korea

<sup>‡</sup>Division of Life Science, Korea Basic Science Institute, Daejeon 305-806, Republic of Korea

<sup>§</sup>Department of Life Science & Chemical Materials, Pohang Accelerator Laboratory, POSTECH, Pohang 790-834, Republic of Korea

---

#### **Techniques and Instrumentations**

Peptide amphiphiles (PAs) were synthesized using CEM Focused Microwave System, Discover (CEM Corporation, North Carolina, USA) and purified by using YL9100 high performance liquid chromatography (HPLC, Younglin, Anyang, Republic of Korea) equipped with a C-18 reverse phase chromatographic column. Mass spectrometry was performed on a Bruker Ultraflex extreme matrix assisted laser desorption/ionization time-of flight/time-of flight (MALDI-TOF/TOF) mass spectrometer (Bruker Daltonik GmbH, Bremen, Germany) using a matrix,  $\alpha$ -cyano-4-hydroxycinnamic acid dissolved in acetonitrile:water = 1:1 mixed solution (0.1% TFA). UV-Vis absorption spectra were obtained from a Shimadzu UV-1800 (Shimadzu, Kyoto, Japan) and NEOSYS-2000 spectrometer (Scinco, Seoul, Republic of Korea). Emission spectra were characterized from a LS-55 (Perkin Elmer, Norwalk, USA) and FS-2 fluorescence spectrometer (Scinco, Seoul, Republic of Korea). Dynamic light scattering (DLS) experiment was performed using ELS-Z (Otsuka Electronics, Osaka, Japan). Attenuated total reflection-Fourier transform infrared (ATR-FTIR) spectra were recorded on ALPHA-P (Bruker Optic GmbH, Bremen, Germany) using ZnSe pellet. Fluorescence microscopy was performed using a Eclipse Ti-E microscope (Nikon, Kobe, Japan). Confocal laser scanning microscopy (CLSM) was conducted by LSM710 (Carl Zeiss, Oberkochen, Germany). Transmission electron microscopy (TEM) images were taken from 300 kV in situ and 120 kV TEM (JEM-3011 HR and JEM-1400, JEOL, Tokyo, Japan, respectively). The secondary structure was determined by a Jasco J-815 circular dichroism (CD) spectrometer (Jasco Inc., Tokyo, Japan) using a quartz

cuvette (path length of ~1 mm) at 20 °C. Two-dimensional (2D) nuclear Overhauser effect spectroscopy (NOESY) was performed on a Bruker AVANCE III 600 nuclear magnetic resonance (NMR) spectrometer (Bruker BioSpin GmbH, Rheinstetten, Germany) equipped with a BBFO broadband probe.  $T_1$  weighted images of  $T_1$  relaxation time of  $Gd^{3+}$ -complexed nanofibrils (NFs) were acquired using a Bruker Biospin 4.7 T scanner (Bruker BioSpin GmbH, Rheinstetten, Germany) with a quadrature birdcage RF coil (with inner diameter of 35 mm).  $T_1$  weighted images were acquired with a conventional spin echo acquisition (TR = 5000 ms) with TE values ranging from 6 to 170 ms. The content of  $Gd^{3+}$  conjugated with NFs was measured by an inductively coupled plasma atomic emission spectrophotometer (ICP-AES, OPTIMA3300DV, Perkin-Elmer, Waltham, USA).

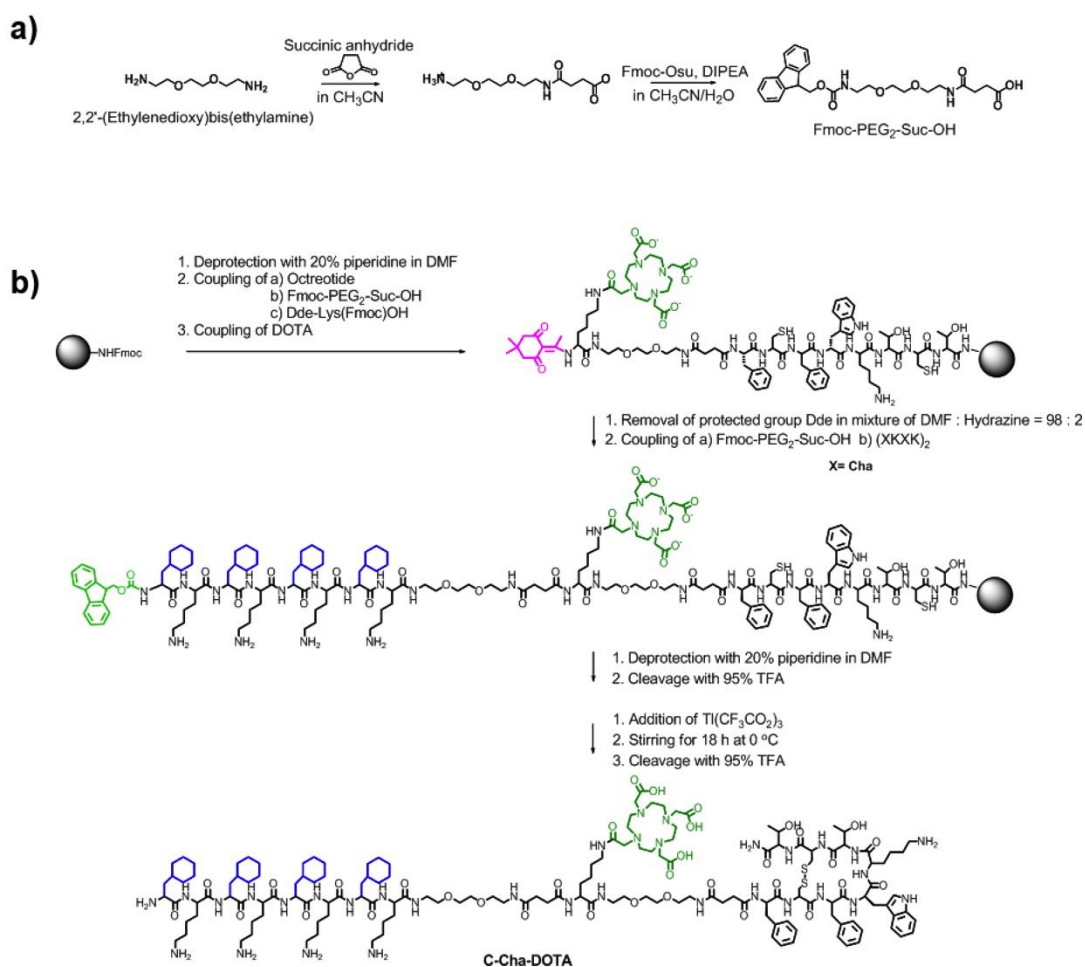


**Figure S1.** Synthesis of a) Fmoc-PEG<sub>2</sub>-Suc-OH<sup>S1</sup> and b) **C-Cha-DOTA**.

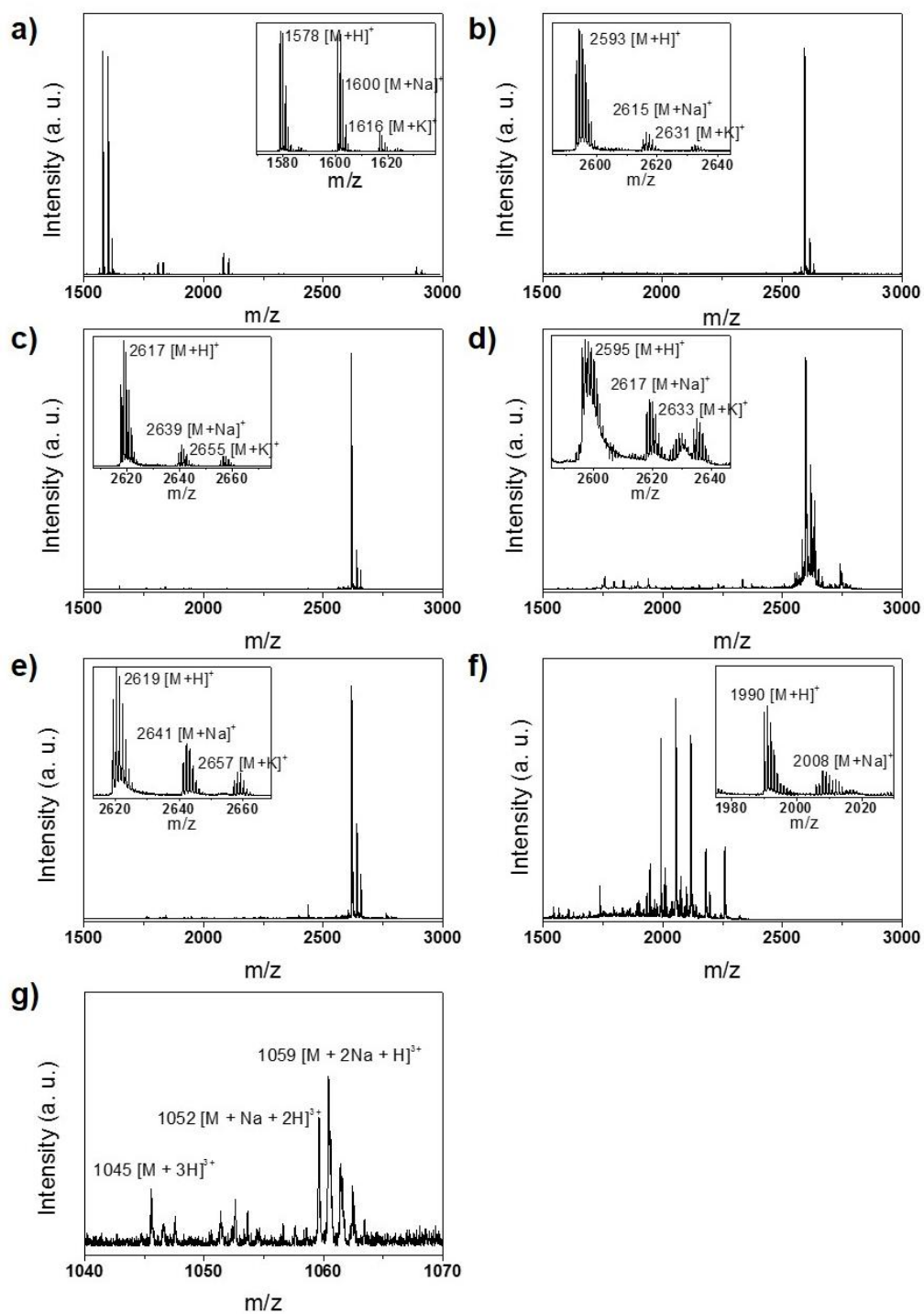


**Figure S2.** MALDI-TOF/TOF mass spectra of PAs: a) N-Phe, b) C-Phe, c) C-Cha, d) A-Phe, e) A-Cha, f) Cha-DOTA, and g) C-Cha-DOTA.

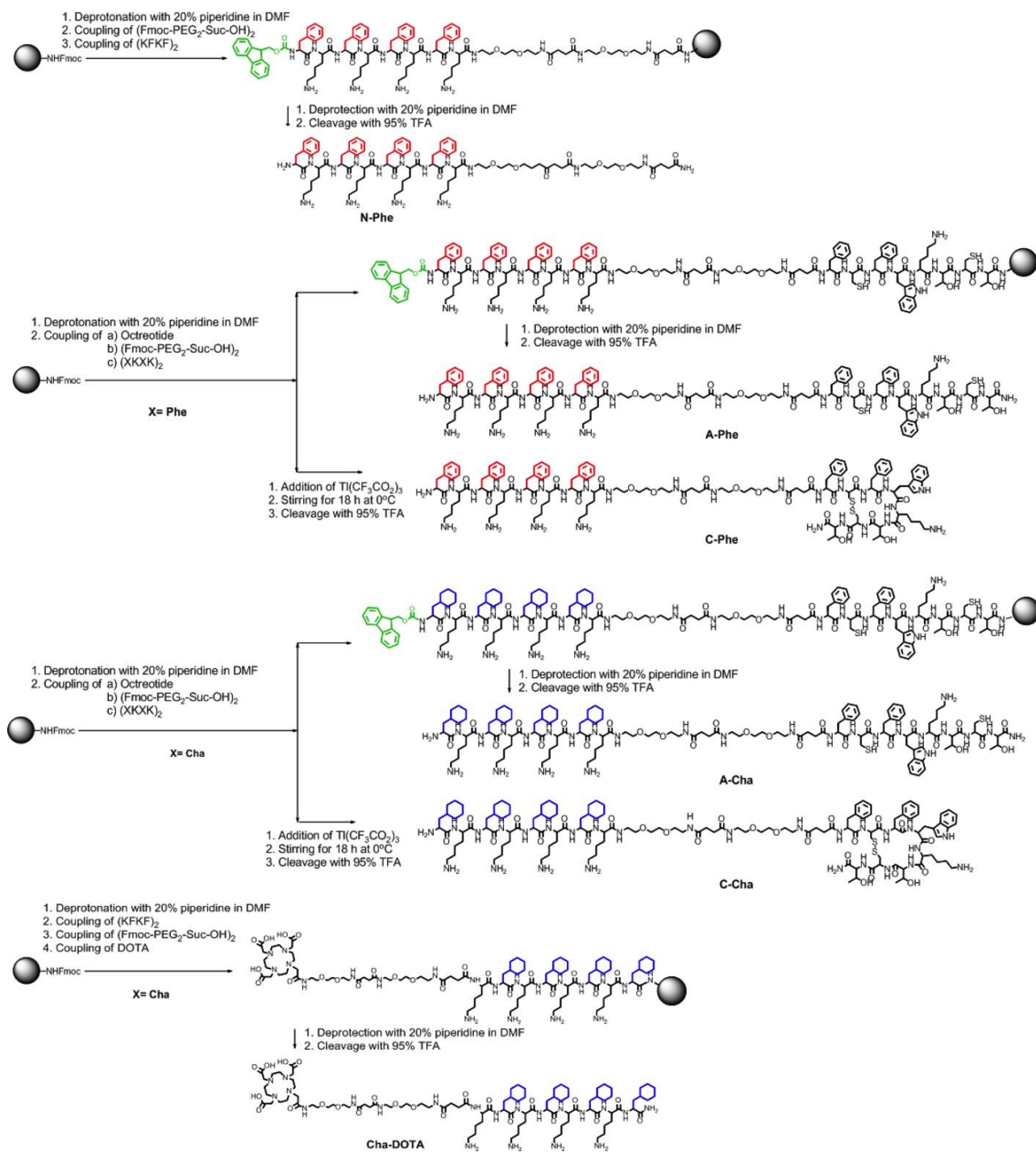


**Figure S3.** Synthesis of PAs.

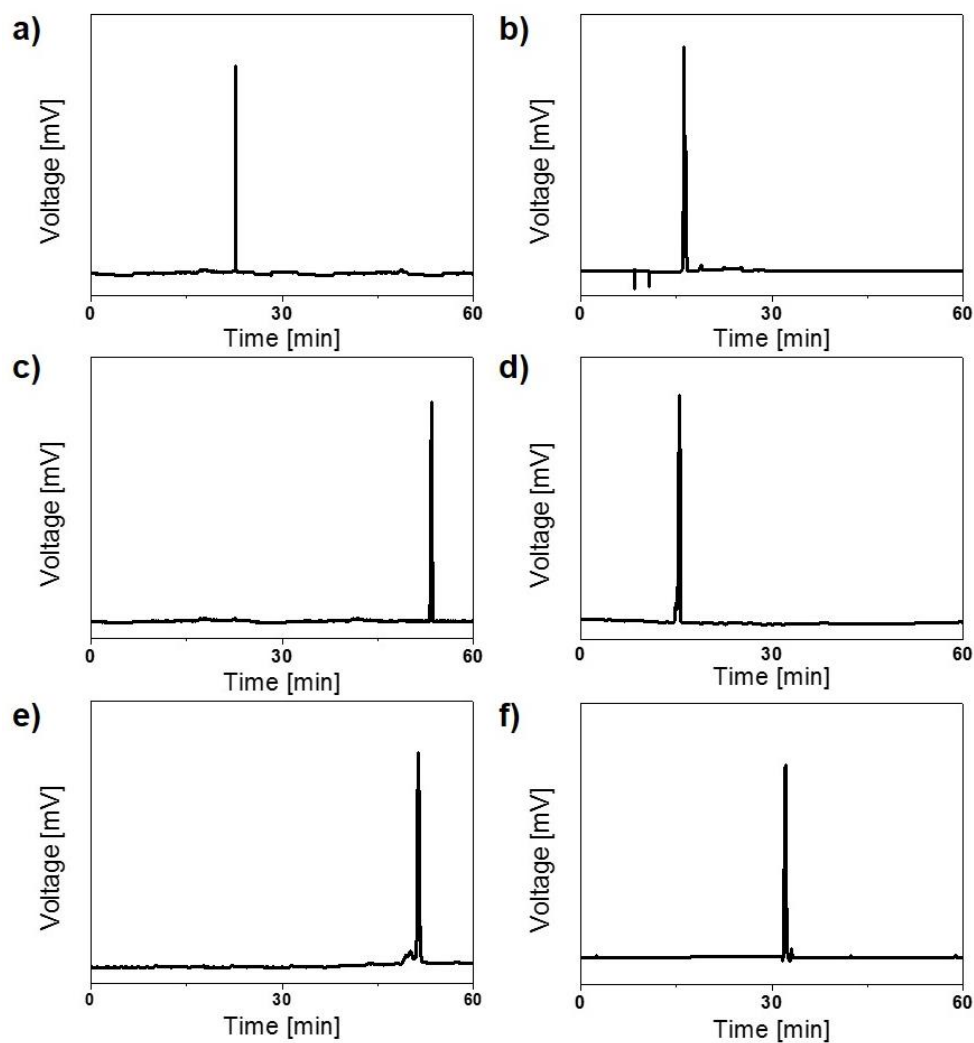


**Figure S4.** HPLC spectra of PAs: a) N-Phe, b) C-Phe, c) C-Cha, d) A-Phe, e) A-Cha, and f) Cha-DOTA.

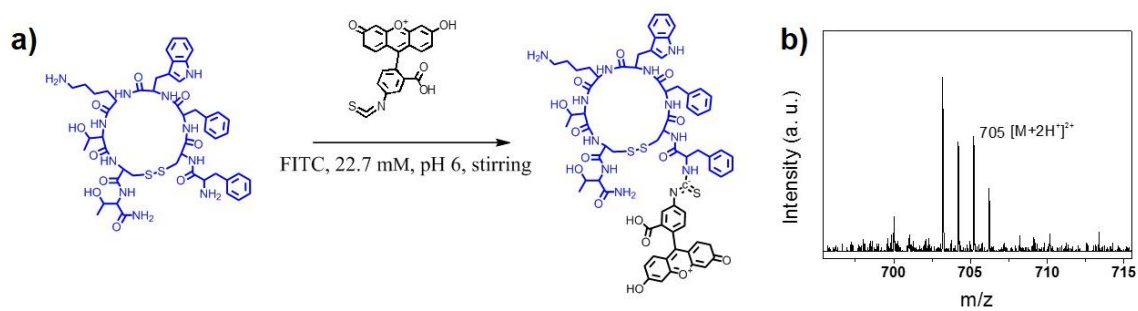


**Figure S5.** a) Synthetic procedure and b) MALDI-TOF/TOF mass spectrum of FITC-labelled octreotide.<sup>S2</sup>

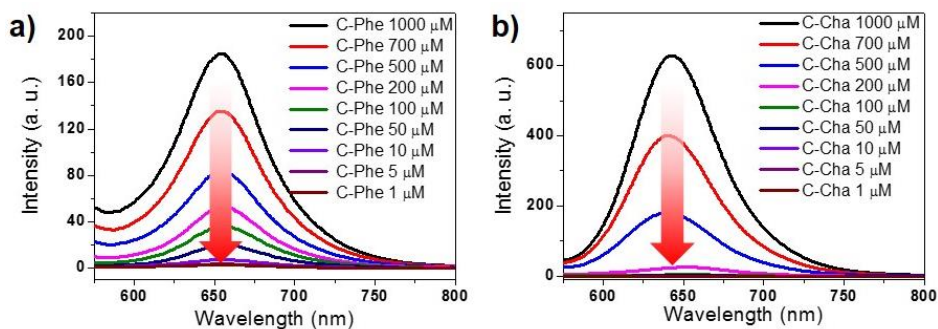


**Figure S6.** Fluorescence intensities of Nile red-loaded a) **C-Phe** and b) **C-Cha** depending on the concentration of PA solutions ( $\lambda_{\text{ex}} = 550$  nm).

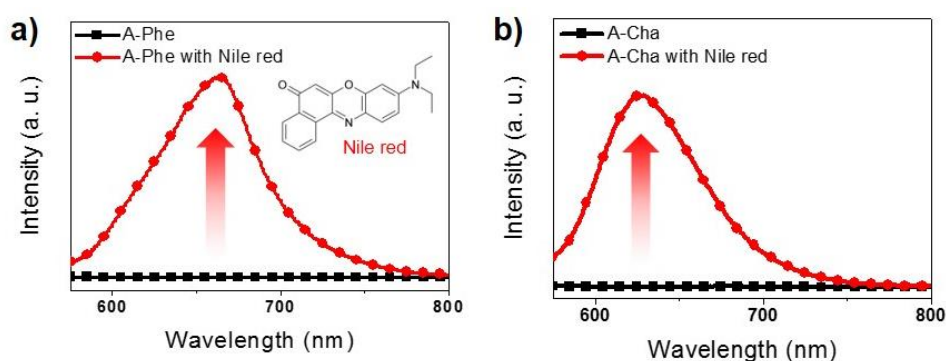


**Figure S7.** Fluorescence spectra before and after encapsulation of Nile red by NFs: a) **A-Phe** and b) **A-Cha** (0.1 mM,  $\lambda_{\text{ex}} = 550$  nm) in 0.1 M NaCl solution.

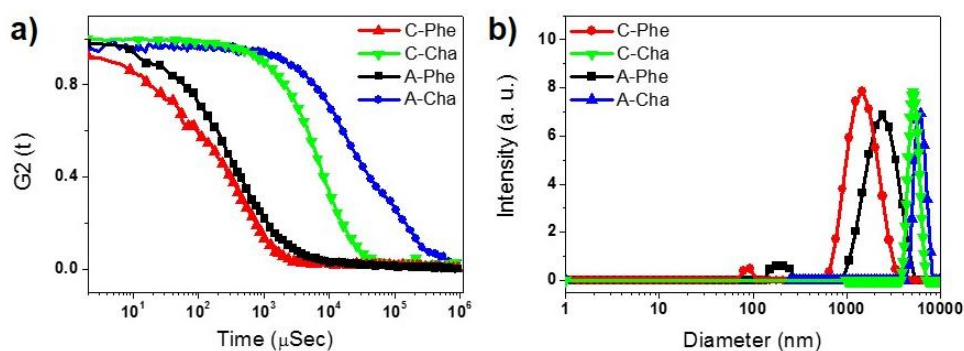


**Figure S8.** DLS measurements of PAs (0.1 mM) in 0.1 M NaCl solution. a) Autocorrelation function by CONTIN analysis and b) hydrodynamic diameters obtained from a).

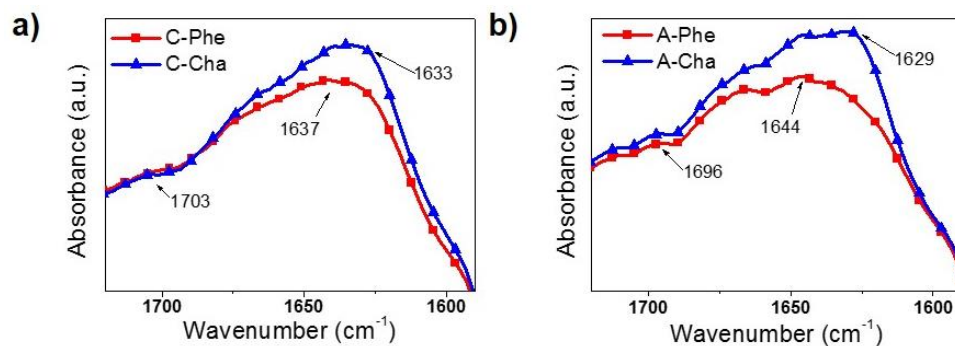


**Figure S9.** ATR-FTIR spectra of PAs (0.1 mM in D<sub>2</sub>O with 0.1 M NaCl solution).

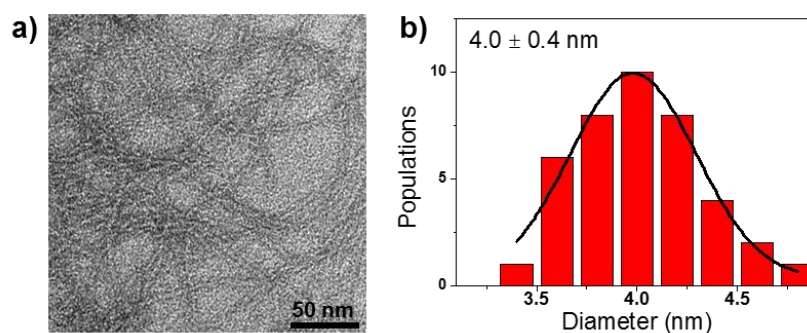


**Figure S10.** a) TEM micrograph showing the self-assembled nanostructures by **N-Phe** (0.1 mM, 0.1 M NaCl solution) stained with 2 wt% uranyl acetate. b) NF diameter distribution for **N-Phe**.

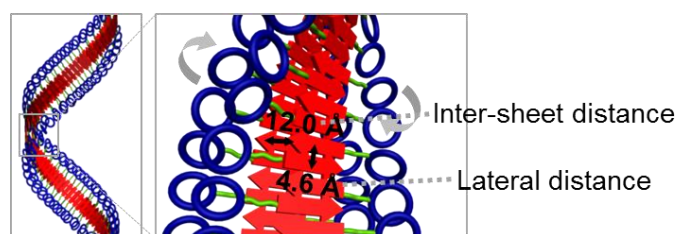


**Figure S11.** Schematic illustration of **C-Cha** with the characteristic distances of  $\beta$ -sheet structure.

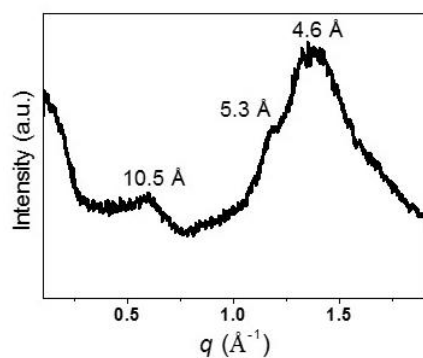


**Figure S12.** WAXS pattern of **C-Phe**. Compared to **C-Cha** shown in Figure 4f, the scattering pattern of **C-Phe** shows additional peak at  $q = 5.3 \text{ \AA}$  which is originated from  $\pi$ - $\pi$  stacking of aromatic side chains of Phe within the self-assembled structures.<sup>S3a</sup> The peaks corresponding to  $d$ -spacing at  $10.5 \text{ \AA}$  and  $4.6 \text{ \AA}$  indicate the formation of  $\beta$ -sheet structure of **C-Phe** with antiparallel alignment, which might arise from the increase in the concentration of PA by solvent evaporation during the sample preparation.<sup>S3b</sup>

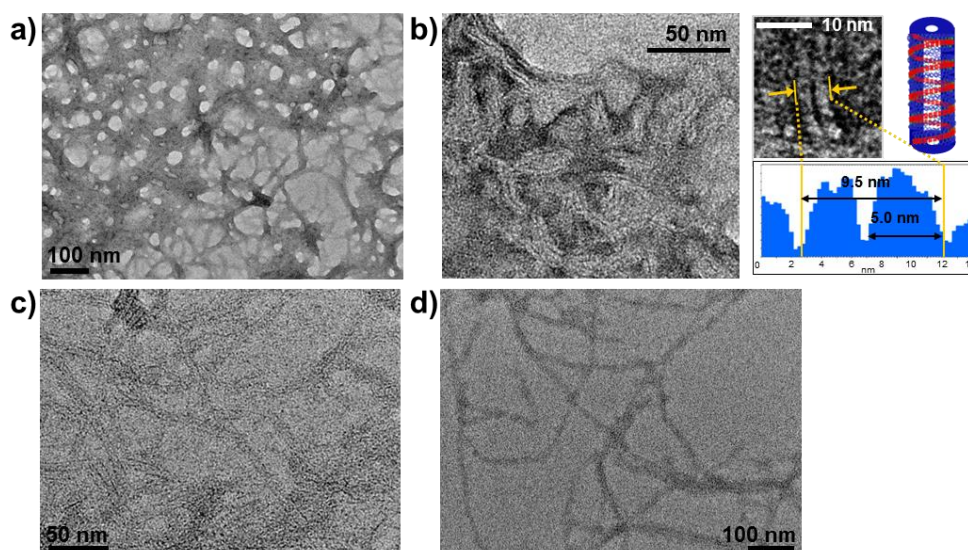


**Figure S13.** Negatively stained TEM micrographs of NFs of a) **C-Phe**, b) **C-Cha**, c) **A-Phe**, and d) **A-Cha** (0.1 mM) after addition of Nile red (2 mol%) in 0.1 M NaCl solution (Inset; density profile indicating the wall thickness of tubular structure of NF). When the aggregates of **C-Cha** containing Nile red were stained with uranyl acetate, which is able to fill the empty space by capillary action, the image showed a dark interior in the elongated objects (as shown in b), indicating the presence of a hollow cavity.

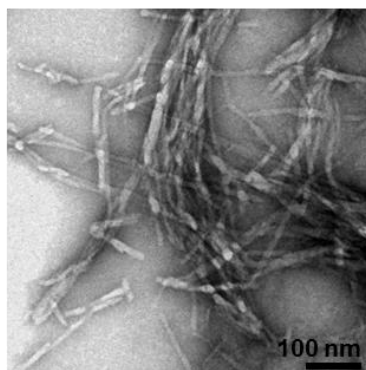


**Figure S14.** TEM micrograph of self-assembled **Cha-DOTA** (0.1 mM) in 0.1 M NaCl solution with negative staining by 2 wt% uranyl acetate.

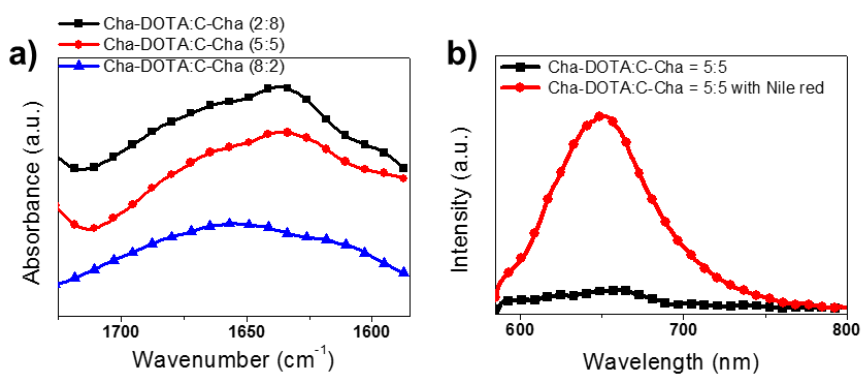


**Figure S15.** a) FTIR spectra of co-assembled nanostructure of **Cha-DOTA** and **C-Cha** with each molar ratio (0.1 mM in D<sub>2</sub>O with 0.1 M NaCl solution). The co-assembled NFs with molar ratios of 2:8 and 5:5 shows the presence of antiparallel  $\beta$ -sheet structure with strong amide I band at 1635 cm<sup>-1</sup> along with weak band at 1682 cm<sup>-1</sup>. b) Fluorescence spectra showing the Nile red-encapsulation capability of aqueous co-assembled nanostructures of **Cha-DOTA** and **C-Cha** with 5:5 molar ratio.



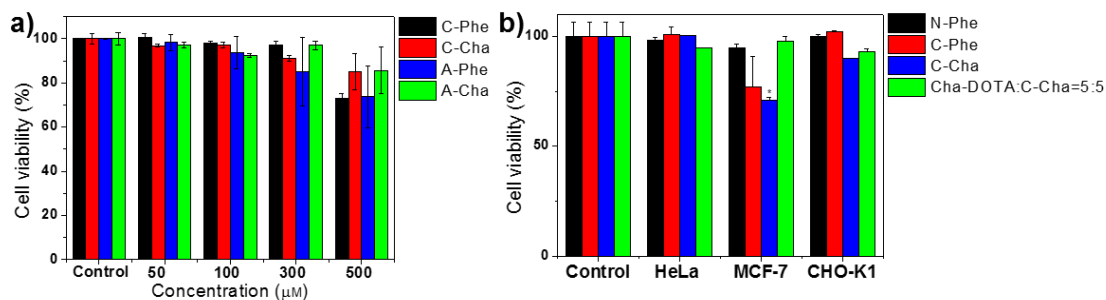


**Figure S17.** Cytotoxicity test of a) various NFs on HeLa cells with different concentrations (50-500 µM), and b) NFs (50 µM) by CCK-8 assay on each cell line after 24 h treatment ( $*p < 0.01$ ).

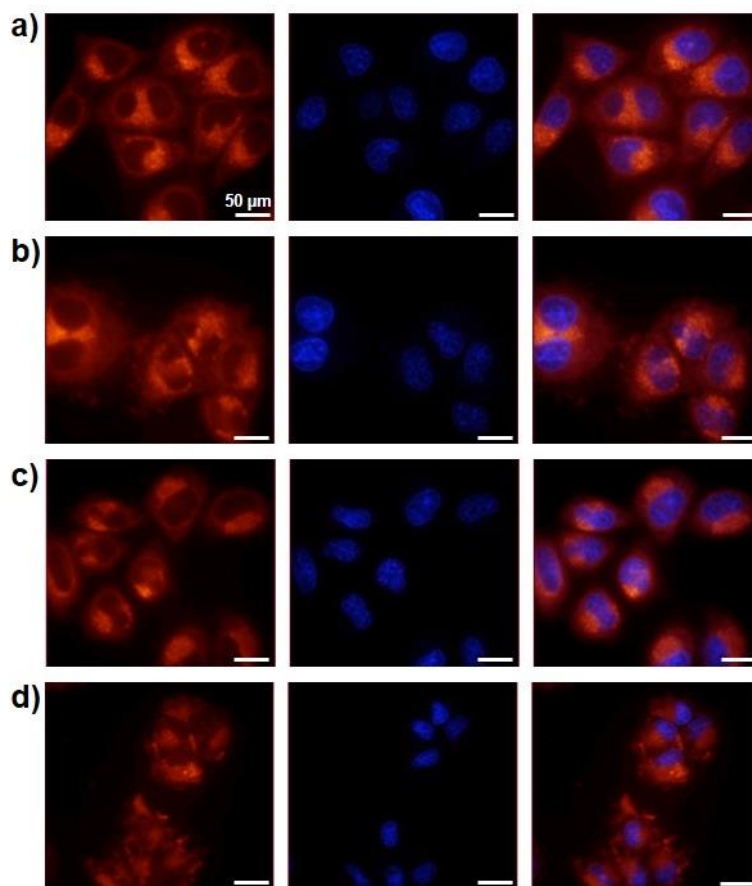


**Figure S18.** Intracellular delivery of Nile red as a hydrophobic drug model. CLSM images of HeLa cells treated with Nile red-loaded NFs (25 µM); a) **C-Phe**, b) **C-Cha**, c) **A-Phe** and d) **A-Cha** for 4 h. Scale bars correspond to 50 µm. For each column, from left to right: Nile red colored red; nuclei stained blue with DAPI; merged images. HeLa cells express high level of somatostatin receptor 2 (SSTR2) that can strongly bind octreotide.<sup>S2,S4</sup>

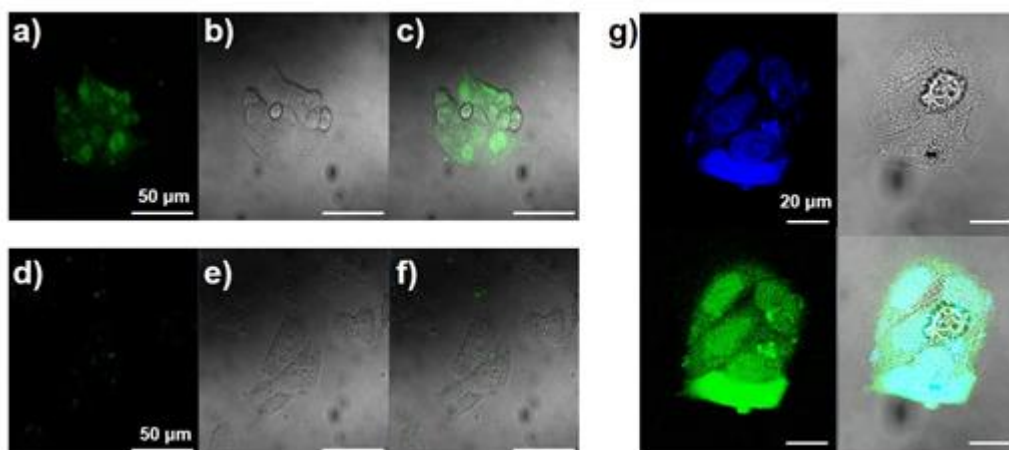


**Figure S19.** Targeting specificity test of octreotide. a,d) Fluorescence, b,e) bright field and c,f) overlay CLSM images of (a-c) MCF-7 and (d-f) CHO-K1 cells after incubation with FITC-labelled octreotide (25  $\mu\text{M}$ ) at 37  $^{\circ}\text{C}$  for 2 h. g) CLSM images of MCF-7 cells treated with FITC-labelled octreotide with higher magnification (25  $\mu\text{M}$ , counterclockwise from top right; bright field image, nuclei stained with DAPI, FITC colored green, merged image). MCF-7 cells overexpress SSTR2 on cell surface while CHO-K1 cells produce much lesser degree of SSTR2.<sup>S4</sup> This data confirms the selective cellular uptake of octreotide by different cell lines depending on the presence of SSTR2.<sup>S2</sup> Green represents the fluorescence of FITC.

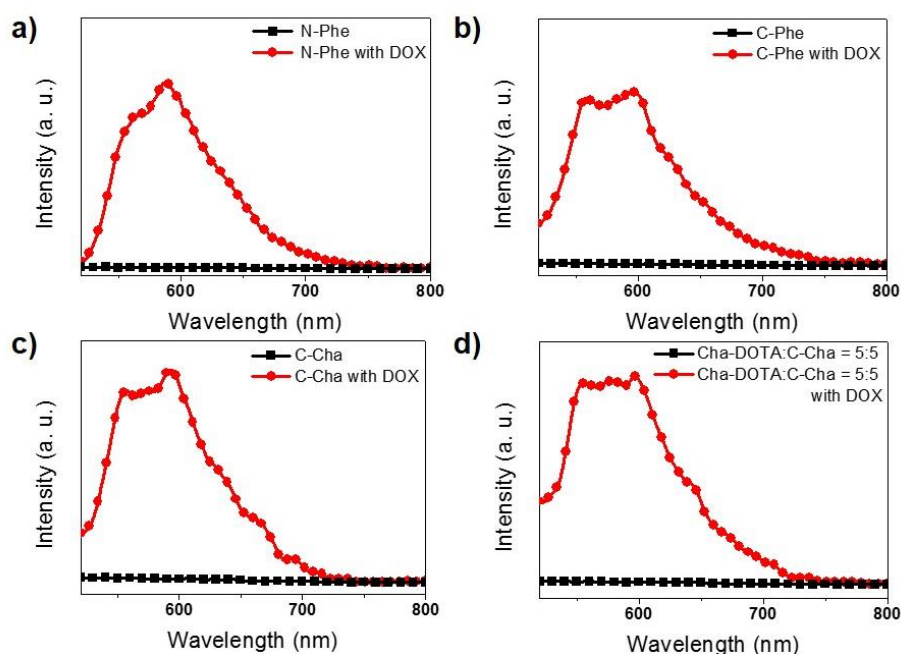


**Figure S20.** Fluorescence spectra before and after encapsulation of DOX by NFs. a) **N-Phe** b) **C-Phe**, c) **C-Cha** and d) **Cha-DOTA:C-Cha = 5:5** (0.5 mM,  $\lambda_{\text{ex}} = 488 \text{ nm}$ ) in aqueous solution.

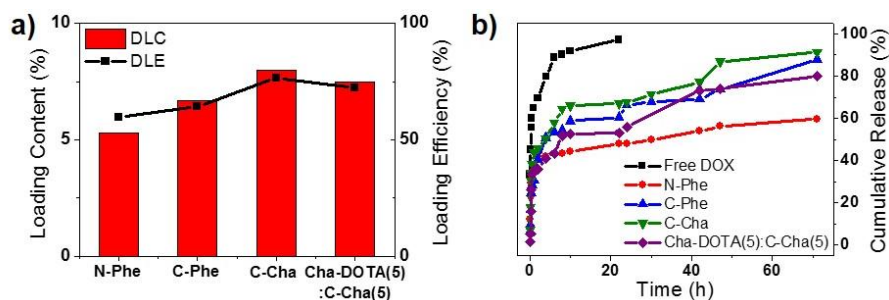


**Figure S21.** a) Drug loading content (DLC) and efficiency (DLE) for DOX-loaded NFs. b) *In vitro* release profiles of free DOX and NFs in sodium acetate buffer of pH 5.5 at 37 °C.

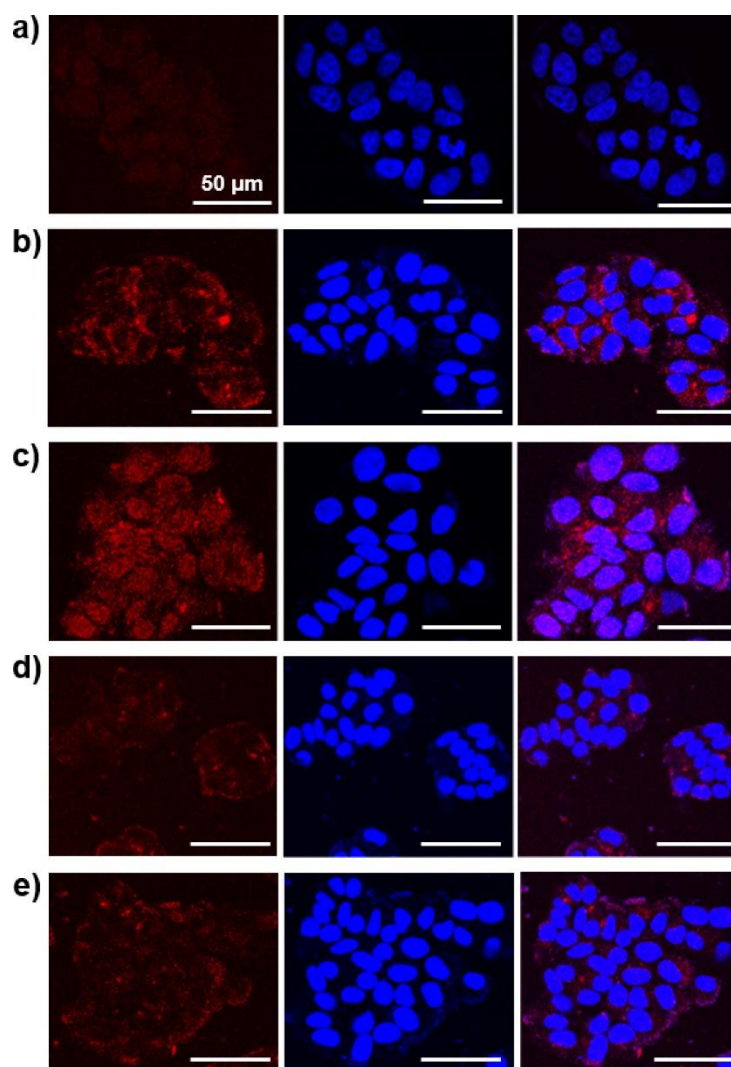


**Figure S22.** CLSM images of MCF-7 cells 24 h treated DOX-loaded a) **N-Phe**, b) **C-Phe**, c) **C-Cha**, d) **A-Phe** and e) **A-Cha** (25 μM). Scale bars correspond to 50 μm. Left: DOX emission in cells (red), middle: nuclei were stained with DAPI (blue), right: merged images.

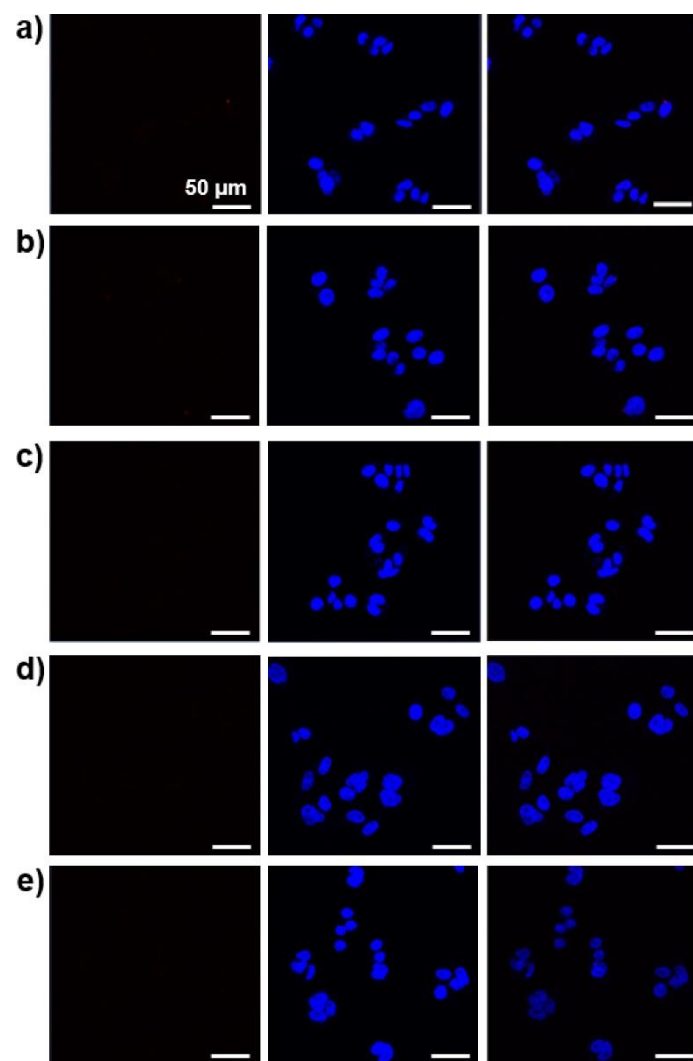


**Figure S23.** CLSM images of CHO-K1 cells 24 h treated DOX-loaded a) **N-Phe**, b) **C-Phe**, c) **C-Cha**, d) **A-Phe** and e) **A-Cha** (25  $\mu\text{M}$ ). Scale bars correspond to 50  $\mu\text{m}$ . Left: DOX emission in cells (red), middle: nuclei were stained with DAPI (blue), right: merged images.

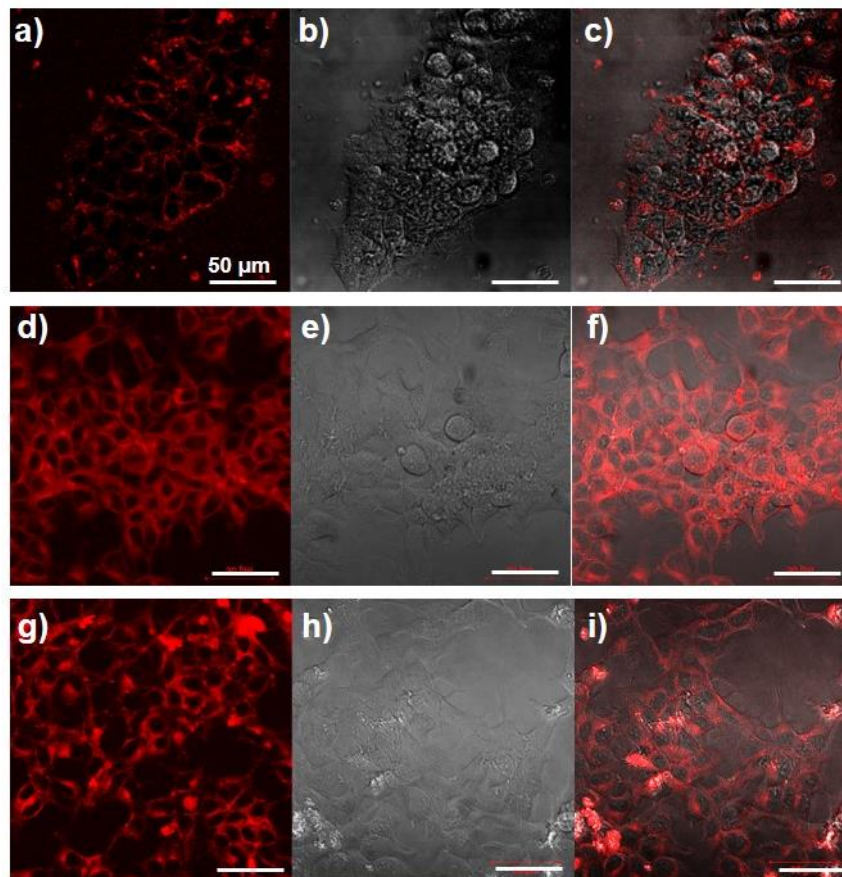


**Figure S24.** Intracellular localization of DOX-loaded NFs of **C-Cha** (25  $\mu\text{M}$ ) in MCF-7 cells imaged by CLSM after incubation of a-c) 30 min d-f) 2 h and g-i) 4 h. MCF-7 cells incubated with DOX-loaded NFs of **C-Cha** exhibited fluorescence of DOX in the membrane as well as cytosol which can be ascribed to the receptor-mediated endocytosis.<sup>S5</sup> Left: fluorescence, middle: bright-field, right: overlay CLSM images.

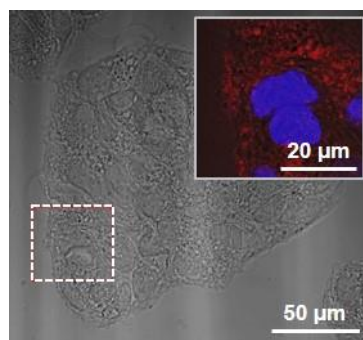


**Figure S25.** CLSM bright field image of MCF-7 cells after 24 h incubation with DOX-loaded NFs of **Cha-DOTA:C-Cha** with 5:5 molar ratio (inset; magnified fluorescence image).

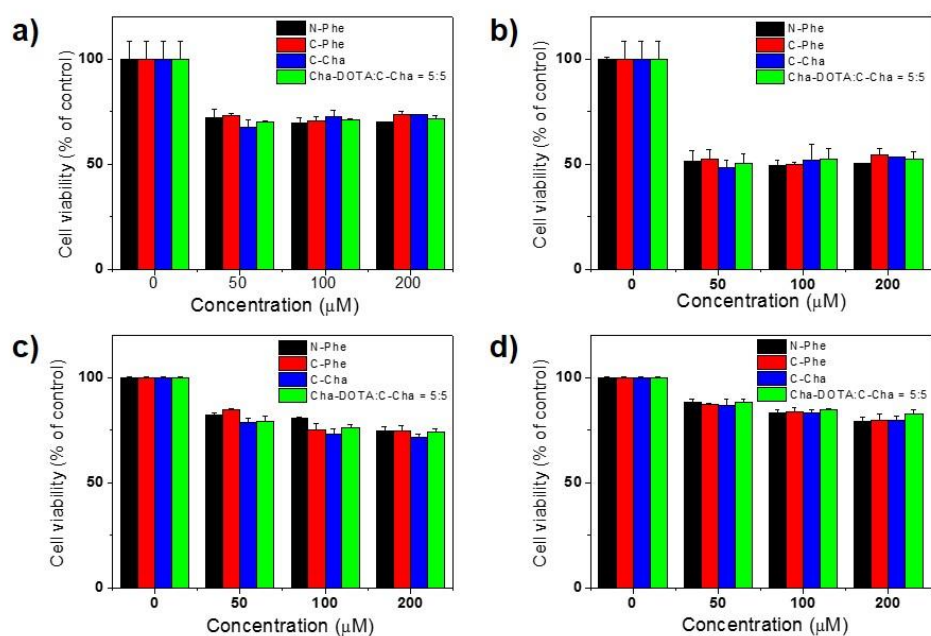


**Figure S26.** Cytotoxicity assay of DOX-loaded NFs (0-200  $\mu\text{M}$ ) in a,b) MCF-7 and c,d) CHO-K1 cells after treatment of 24 h (left) and 48 h (right).

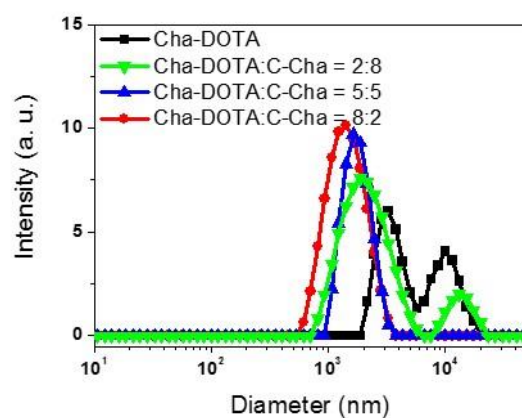


**Figure S27.** Hydrodynamic diameters of co-assembled NFs in 0.1 M NaCl solution as determined by DLS (0.1 mM).

## References

- S1. Song, A.; Wang, X.; Zhang, J.; Mařík, J.; Lebrilla, C. B.; Lam, K. S. *Bioorg. Med. Chem. Lett.* **2004**, *14*, 161-165.
- S2. Abdellatif, A. A. H. *Biochem. Physiol.* **2015**, *4*, 1000183.
- S3. a) Banerjee, A.; Palui, G.; Banerjee, A. *Soft Matter* **2008**, *4*, 1430-1437; b) Behanna, H. A.; Donners, J. J. J. M.; Gordon, A. C.; Stupp, S. I. *J. Am. Chem. Soc.* **2005**, *127*, 1193-1200.
- S4. Tian, X.; Baek, K.-H.; Shin, I. *Chem. Sci.* **2013**, *4*, 947-956.
- S5. Lelle, M.; Kaloyanova, S.; Freidel, C.; Theodoropoulou, M.; Musheev, M.; Niehrs, C.; Stalla, G.; Peneva, K. *Mol. Pharmaceutics* **2015**, *12*, 4290-4300.